ISFV13 - 13th International Symposium on Flow Visualization
FLUVISU12 - 12th French Congress on Visualization in Fluid Mechanics
July 1-4, 2008, Nice, France

INVESTIGATION OF THE FLOW IN A CIRCULAR CAVITY USING STEREO AND TOMOGRAPHIC PIV

Haigermoser C.*, Scarano F. **, Onorato M.*
***Politecnico di Torino, Italy.**
**** TU Delft, The Netherlands.**

KEYWORDS:
Main subject(s): *Circular cavity flow*
Fluid: *Cavity flow, circular, turbulent boundary layer, asymmetric flow*
Visualization method(s): *PIV*
Other keywords: *stereo PIV, tomographic PIV*

ABSTRACT : *In the present paper the flow over a circular cavity with an aspect ratio of D/H = 2 and with a turbulent upstream boundary layer is studied. The scope of the investigation is the asymmetrical flow pattern occurring for certain cavity aspect ratios D/H and inflow conditions. The flow field is measured in a vertical and several wall-parallel planes using stereo PIV, giving a statistical flow description. The tomopraphic PIV measurements give insight into the instantaneous 3D flow inside the cavity. The asymmetric flow pattern is observed, consisting of a steady vortex, placed diagonally inside the cavity. The cavity's shear layer is dominated by two types of structures, the ones originating from the instabilities of the separated shear layer and those already present in the turbulent boundary layer prior to separation.*

1 Introduction

Cavity flows are of high interest in engineering applications, such as wheel wells, fuel vents on aircrafts or cavities between train wagons. In these examples, cavities show to be a considerable acoustic noise source, and especially for increasing Mach number, they can also lead to significant structural loads. It is therefore necessary to understand such flows and find means to control them.
Furthermore, cavity flows offer a broad range of fluid mechanical phenomena, like a unsteady shear layer developing from the leading edge, vortex shedding, recirculation zones, instability and 3-dimensional effects. These phenomena play a role in the cavity flow, even using such a simple geometry.
Generally, cavity flows are distinguished based on several characteristics, where the two most important are the geometrical form of the cavity and the upstream boundary layer. Most of the studies up to date have been concerned with rectangular cavity flows and only a few with the flow in a circular cavity.
The scope of this paper is the investigation of the flow in a circular cavity with a diameter to depth ratio D/H = 2, where several previous studies revealed that the flow in the cavity becomes asymmetric, which is connected with an increase in drag with respect to other aspect ratios. More precisely, Hiwada et al. (1983) [1] investigated the surface pressure distribution on the cavity walls for aspect ratios $1 < D/H < 10$ and found the flow being stable and symmetric for $D/H > 5$ and $D/H < 1.25$. Instead for

2.5 < D/H < 5 the flow becomes unstable and a shear layer flapping was observed. For 1.4 < D/H < 2.5 the flow becomes asymmetric. This asymmetry is bi-stable, meaning that a forced disturbance can change the orientation of this phenomenon. Besides others, Dybenko et al. (2006) [2] confirmed these results with surface pressure measurements and hot-wire measurements in the cavity wake. Additionally, they performed acoustic measurements, which revealed a peak in the acoustic spectra for D/H ≈ 0.5, which was not present at other aspect ratios. The frequency was close to the one predicted by the Rossiter [3] formula, whereas the frequencies at the other aspect ratios where well predicted by an equation based on the Helmholtz resonance tone [4]. Dybenko et al. conclude that the asymmetric flow is somehow related to the occurrence of an acoustic feedback mechanism.
Rona 2007 [5] developed an analytical model to investigate oscillations in circular cavities. At aspect ratios of 0.71 and 2.5 asymmetric flow modes were predicted, corresponding to the above experimental investigations.
The mentioned studies of cylindrical cavity flows give an estimation of the 3-dimensional flow pattern inside the cavity, but a direct measurements of the flow pattern is still missing. The paper will present an experimental investigation using stereo and tomographic PIV in order to clarify the flow pattern with the before mentioned cavity configuration.

2 Experimental Setup

The experiment was conducted at the Aerodynamics Laboratories of TU Delft in a open wind tunnel with a test section area of 400x400mm^2. A flat plate was placed upstream of the cavity to control the development of the upstream boundary layer, which was tripped at the flat plate's leading edge with a strip of sand paper. The plate was placed into the test section center so that the cavity was situated right at the test section exit in order to enable optical access, see Fig. 1.

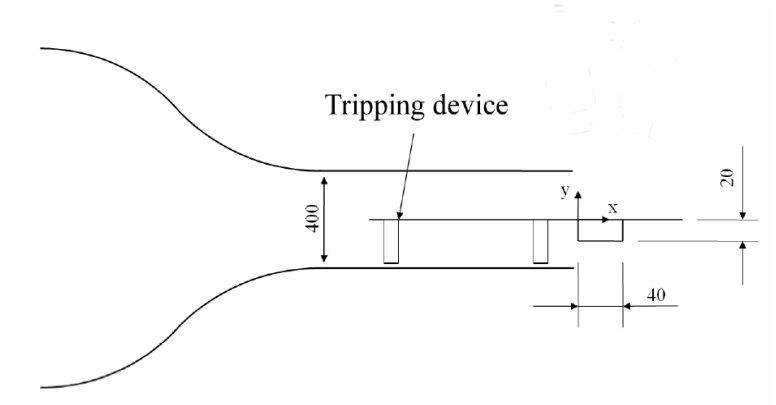

Fig. 1. Experimental setup; units in mm; not in scale.

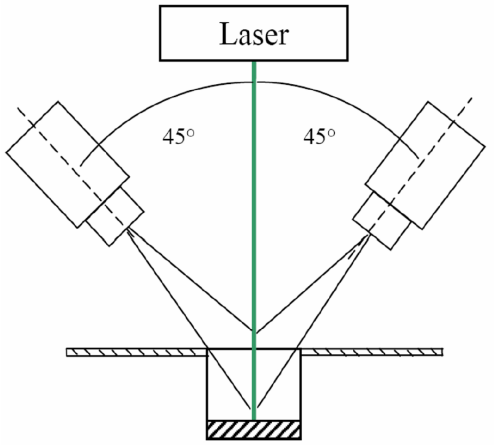

Fig. 2. Stereo PIV setup in vertical plane.

The cavity's upstream boundary layer was fully turbulent with the characteristics as shown in table 1. The ratio of the boundary layer thickness and the cavity depth was δ/H=1.125 and was deemed to be large to produce a regular vortex shedding due to shear layer instabilities. An important parameter which determines the occurrence of oscillations in a cavity is the ratio of the cavity length (respectively diameter) D over the boundary layer momentum thickness θ. This ratio is here 14, which is low with

respect to values found in literature for rectangular cavities, above which cavity flow oscillations are expected.

U_e[m/s]	δ[mm]	θ[mm]	Re_L	D/θ	δ/H
12	22.5	2.8	31000	14	1.125

Table 1. Incoming boundary layer characteristics.

The experiments were conducted by 2 (for stereo PIV) and 4 (for tomographic PIV) PCO Sensicam QE CCD cameras (1376x1040 pixels). The cameras were equipped with Nikon lenses with a focal length of 60mm at $f_{\#}$=8. The measurement plane, respectively the measurement volume was illuminated by BigSky CFR200 Nd:YAG laser with a maximum energy of 200mJ per pulse and a maximum repetition rate of 30Hz. Oil droplets with a diameter of 1 µm were used to seed the flow, yielding a particle image diameter of approximately 3 pixels. Before correlating the images, a background image was subtracted from the PIV images to reduce reflections coming from the cavity walls.
Three kinds of experiment were carried out:
a) Stereo PIV measurements in the vertical streamwise (x-y) plane in the middle of the cavity.
b) Stereo PIV measurements in different horizontal streamwise (x-z) planes, placed at different heights along the cavity axis.
c) Tomographic PIV measurements in the upper half of the cavity.
For the stereo PIV measurements in the vertical plane, the 2 cameras were placed as shown in Fig. 2. The field of view covered the whole cavity and the outer flow (-20mm< x<20mm;-20mm< y <20mm). The images were analyzed with the LaVision Davis 7.3 software, using a multi-step cross-correlation with a final interrogation window size of 32x32 pixels (0.9x0.9mm^2) with 50% overlap. The datasets used for statistical evaluation comprised 800 snapshots.

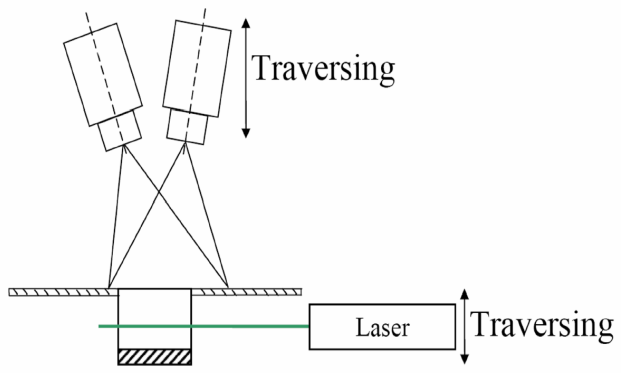

Fig. 3. Stereo PIV setup in horizontal plane.

For the stereo PIV measurements in the horizontal planes, the two cameras were placed above the cavity with an angle of 10° with respect to the cavity axis, and they were fixed onto a vertically traversing rigid structure. The camera angles are low to obtain a good estimate of the out-of-plane velocity component, but higher angles would have reduced the field of view, especially for planes deeper inside the cavity (Fig. 3). The field of view was 60x44mm^2 and included the cavity and a part downstream.

The laser light sheet was introduced laterally through the cavity side walls, which made it necessary to build them as thin as possible, in order to minimize the refraction of the light sheet and to insure a homogeneous illumination of the particles inside the cavity (Fig. 3).
The measurements were performed at 12 different wall-normal positions spaced between -17mm < y < 8mm, by moving the laser and the cameras along the wall normal direction. The images

were cross correlated using the same type of algorithm as in the vertical stereo measurements, see above. Here, one vector represents the mean velocity in a area of 1.4x1.4mm^2. At each location 300 instantaneous velocity fields were obtained. The stereoscopic system was calibrated outside the cavity with a 2-level calibration target and the calibration was corrected at each level using a self-calibration procedure, see Wienecke (2005) [8].
The tomographic PIV experiment was carried out adding two cameras to obtain a total of 4 views all inclined 10° from the cavity axis. The laser light sheet was expanded to a thickness of 8mm. The measured volume was located at -10mm < y < -2mm. The images were pre-processed subtracting the background using images captured without introducing any seeding. Further, the particle image intensity was equalized and pixel noise was reduced by Gaussian smoothing. The volumes were reconstructed using 5 MART iterations (see next section) at a pixel to voxel ratio of 1 leading to a volume of 1094x1088x224 voxels (24 voxels per mm). The reconstructed volumes were cross-correlated using the VODIM software developed at the TU Delft. The final interrogation volume size was 30x30x30 voxels (1.6x1.6x1.6mm^3) at an overlap of 50%.

3 Tomographic PIV - Working Principle

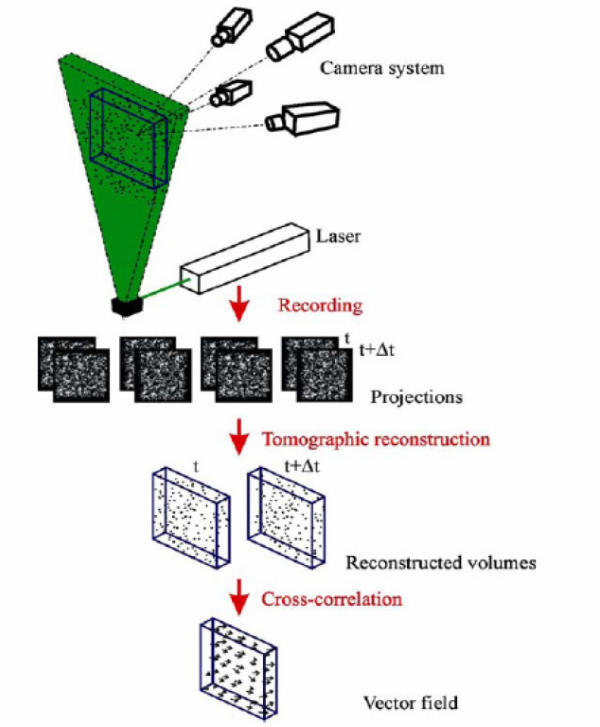

Fig. 4. Working principle of tomographic PIV.

This section gives a quick overview on tomographic PIV. For details it is referred to Elsinga et al. 2006 [6] and Elsinga et al. 2006 [7]. The working principle is shown in Fig. 4 (Figure from [7]). A fluid volume seeded with particles is illuminated with a thick laser light sheet. Two successive images are recorded simultaneously with four cameras as it is done in stereo PIV. In the successive step one has to obtain the 3D distribution of the particles in the volume from the 4 images. Here comes in the new part of the technique, the tomographic reconstruction. It was seen that a algebraic iterative algorithm was most appropriate for the reconstruction. The Multiplicative Algebraic Reconstruction Technique (MART) assumes a light intensity distribution E(X,Y,Z) divided in voxels and relates it to the pixel intensity I(x,y) obtained from the cameras via a weighting factor $w_{i;j}$:

$$\sum_{j \in N_j} w_{i,j} E(X_j, Y_j, Z_j) = I(x_i, y_i) \qquad (1)$$

where the index i referes to the camera pixels and j refers to the voxels in the volume. The voxel intensity E(X,Y,Z) is updated in every iteration:

$$E(X_j,Y_j,Z_j)^{k+1} = E(X_j,Y_j,Z_j)^k \left(\frac{I(x_i,y_i)}{\sum_{j\in N_j} w_{i,j} E(X_j,Y_j,Z_j)^k} \right) \quad (2)$$

Having obtained the 3D light distribution a 3D cross-correlation algorithm is used to calculate the velocity vectors in the volume, similar to a 2D cross-correlation.
The time to obtain one reconstructed volume was approximately 1 hour on a quad-core PC. The 3D correlation required about the same time.

4 Stereo PIV results

4.1 Vertical plane

The mean velocity field from the measurements in the vertical symmetry plane (Fig. 5) shows a recirculation zone occupying the whole cavity. The asymmetry of the flow is indicated by the out of plane velocity component.

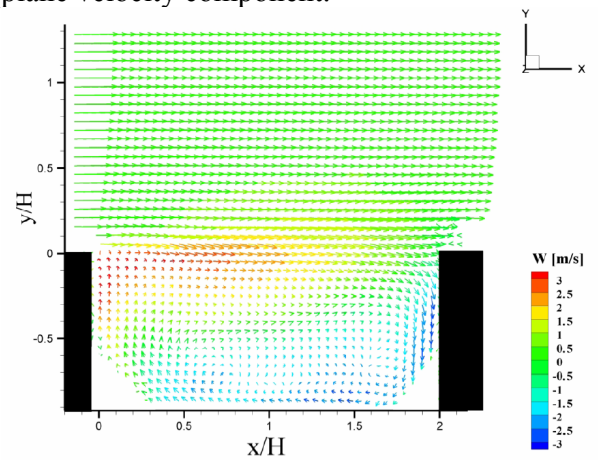

Fig. 5. Mean velocity field in the plane of symmetry; vector color coded by out of plane velocity component W.

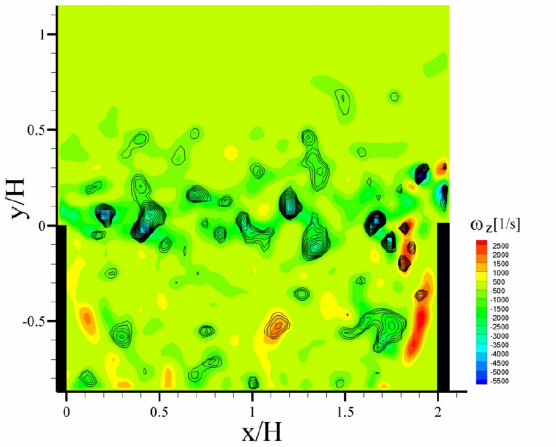

Fig. 6. Instant flow field. Color plot: vorticity ω_z; isolines: λ_{ci}..

One notices the flow going in positive z direction close to the upper corner at the cavity's leading edge and going in negative z-direction close to the bottom at the trailing edge. Moreover, in the middle of the cavity mouth respectively in the shear layer, the W velocity component shows to be positive. Thus, the asymmetric motion in the cavity is strong enough to influence the zones of high momentum in the shear layer, which may explain the high drag coefficient, which is found for asymmetric circular cavity

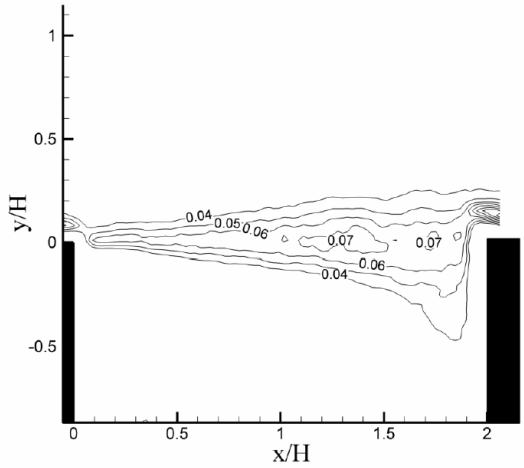

(a) U_{RMS}/U_e.

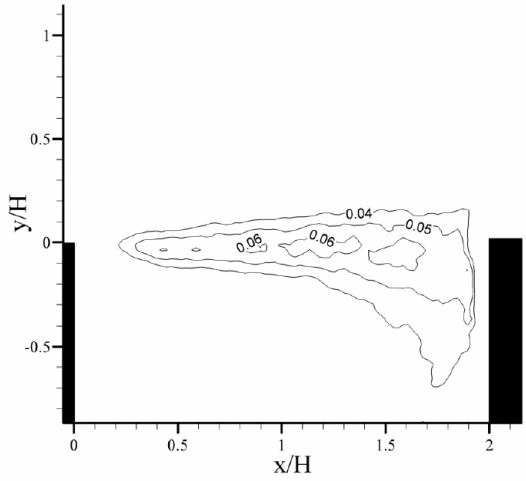

(b) V_{RMS}/U_e.

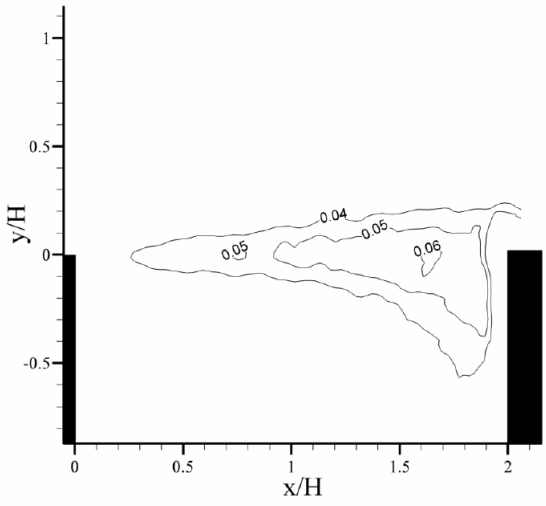

(c) W_{RMS}/U_e.

Fig. 7. Normalized velocity RMS levels.

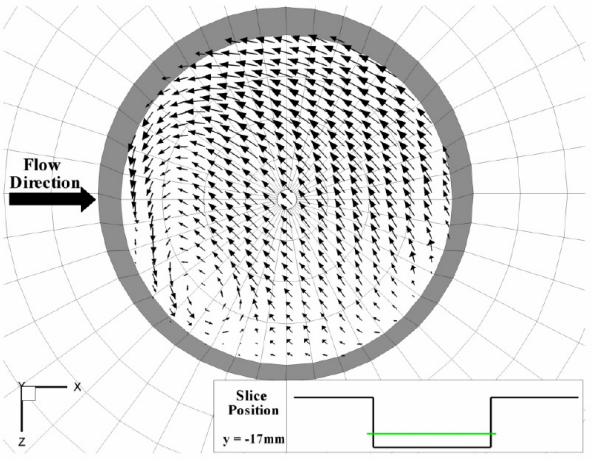

(a) y = -17mm.

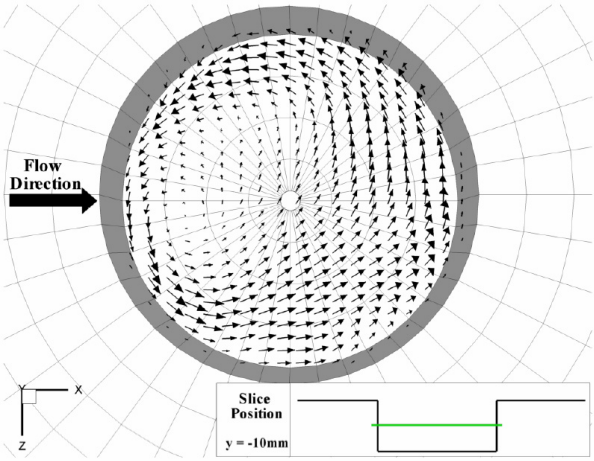

(b) y = -10mm.

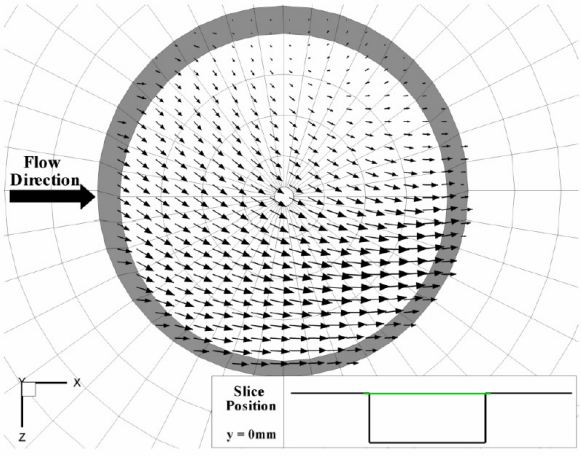

(c) y = 0mm.

Fig. 8. Mean velocity vector fields.

flows. Fig. 6 shows a plot of the instant vorticity ω_z and λ_{ci} isolines identifying vortices [9]. As expected because of the low D/θ ratio, an irregular vortex shedding is seen from the leading edge. For regular vortex shedding the flow pattern would show a more regular spacing of the vortices in the shear layer. Apparently, due to the thick boundary layer, the shear stresses in the shear layer are not high enough to induce regular instability mechanisms. Instead, it is assumed that the flow structures of the incoming boundary layer dominate the shear layer instability mechanism. It must be pointed out that these observations are only visual and to clearly determine weather the vortex shedding is regular or not, time-resolved data would be necessary.

In Fig. 7 a-c the RMS values of the three velocity components normalized with the free stream velocity Ue are shown. In all figures a similar pattern is observed, which is also known from rectangular cavity flows.

More downstream, the fluctuations grow in amplitude and the region spreads in wall-normal direction. The maximum of the normalized RMS values for the U and V component is found at $x/H \approx 1.25$ with values of 0.07 and 0.06, respectively. Again, this location of the maxima is close to locations found in rectangular cavity flows. The maximum of the W-component is located more downstream at $x/H \approx 1.75$ and assumes a value of 0.06. Moreover, the contour levels indicate an entrainment of the fluctuations of all components into the cavity at its trailing edge due to the asymmetric flow, a feature which is not observed for symmetric cavity flows. In the remainder, we will denote with ”upper” the area of the cavity where $z < 0$ located in the top of the images, whereas “lower” refers to $z > 0$.

Fig. 8a-c show the mean velocity field obtained from the stereo PIV measurements in the planes parallel to the wall at y = -17mm, y = -10mm and y = 0mm. In Fig. 8a a recirculation zone is observed with its center close to the upstream end. Upwards, this recirculation center is displaced in clockwise direction and disappears outside the cavity. Further, Fig. 9 shows that fluid is enters into the cavity in the ”lower” downstream area and exits from it at the opposite side. This is visualized by the vertical velocity component (color code of vectors). This condition applies to all observed planes.

The 3-dimensional mean flow pattern is visualized in Fig. 10. The streamlines indicate an anticyclone like recirculation zone starting at the ”lower” upstream part of the cavity bottom. It exits the cavity in the ”upper” downstream area, where the center of the recirculation zone (Fig. 8c) is not visible any more due to the horizontal orientation of the vortex core line. Hence, the anticyclone is placed asymmetrically inside the cavity and it’s dimension is comparable to the cavity dimensions. This result agrees with the conceptual sketch proposed by [1]. In Figs. 11, 12 and 13 the RMS values of the different velocity components normalized with the free stream velocity U_e are shown at 4 different y-positions. Comparing the obtained normalized RMS values in the x-y-plane in the middle of the cavity (Figs. 11-13) with the values from Fig. 7 it is seen that the V component shows slightly higher values in the horizontal measurements with ascribed to the higher uncertainty when measuring the out-of-plane component with the stereo PIV setup. The other 2 components assume similar values like in the vertical measurements. It is seen that in the center of the recirculation zone (Fig. 8a together with Fig. 11a and Fig. 12a) the RMS values are lower with respect to the outer part of the vortex. This feature is still visible in the next higher level (Fig.s 11b-13b), where additionally high turbulence activity is found close to the downstream side wall, which is due to the downwards deflection of the flow (see color code in Fig. 9). At y=-3mm (Figs. 11c-13c) high velocity fluctuations are observed at the ”lower” downstream part, where the flow is entering from the boundary layer into the cavity. Instead, at y = 4mm in Fig. 11d high values of $U_{rms}=U_e$ are found were the flow exits the cavity in the ”upper” downstream part and interacts with the incoming boundary layer.

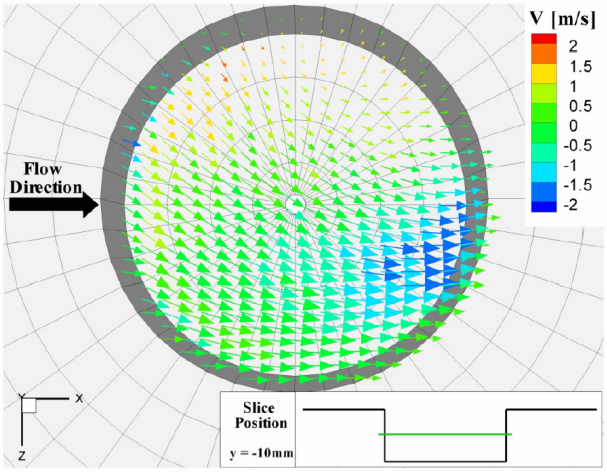

Fig. 9. Mean Velocity Field at y = -10mm. Vector color coded by out of plane velocity component V.

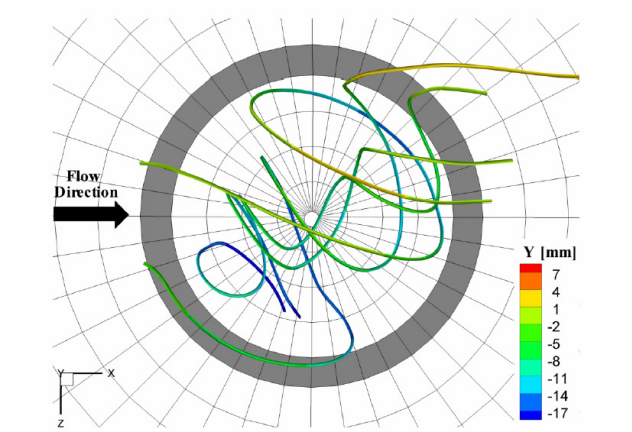

(a) Top view. Streamline color coded by y-coordinate.

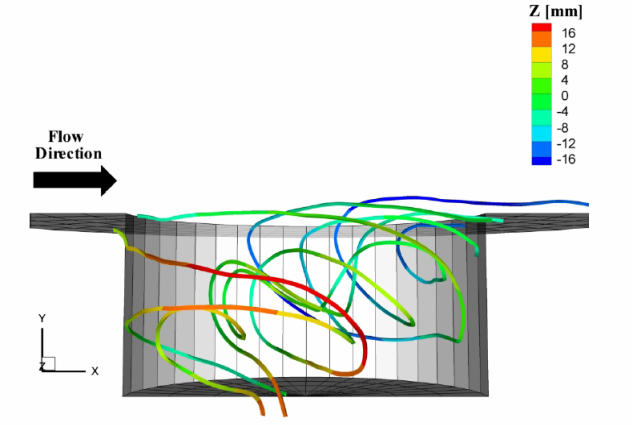

(b) Side view. Streamline color coded by z-coordinate.

Fig. 10. Streamlines.

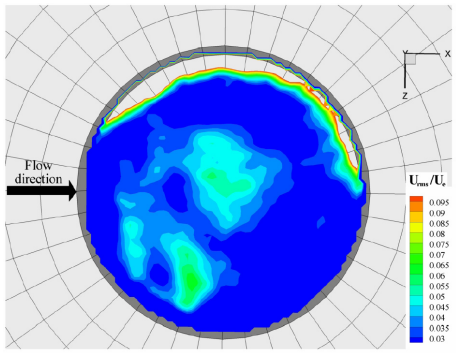

(a) y = -17mm.

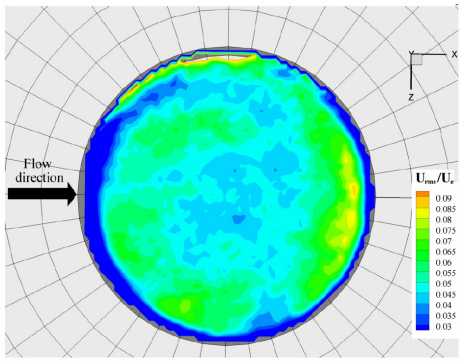

(b) y = -10mm.

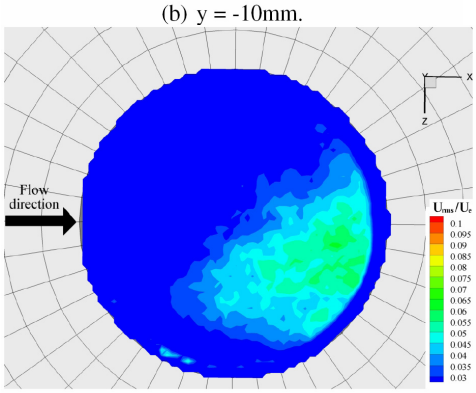

(c) y = -3mm.

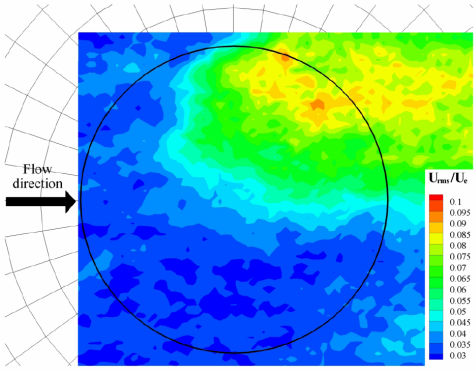

(d) y = 4mm.

Fig. 11. RMS values of U-velocity in different horizontal planes.

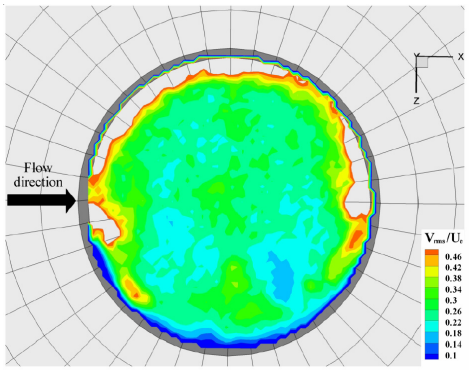

(a) y = -17mm.

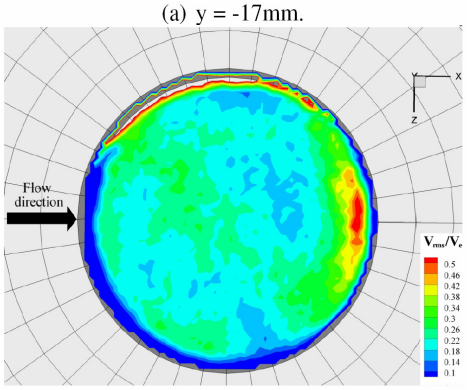

(b) y = -10mm.

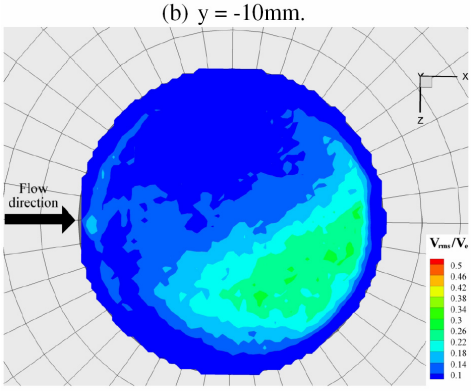

(c) y = -3mm.

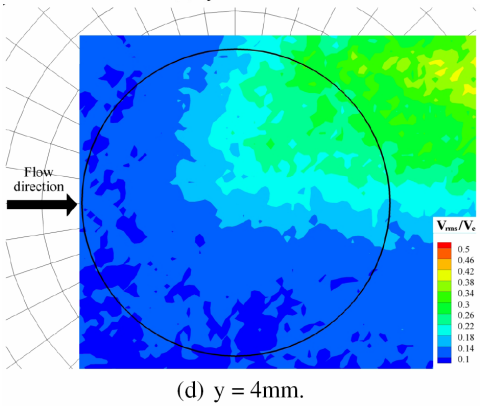

(d) y = 4mm.

Fig. 12. RMS values of V-velocity in different horizontal planes.

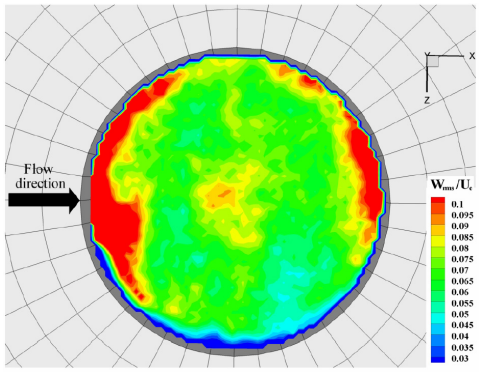

(a) y = -17mm.

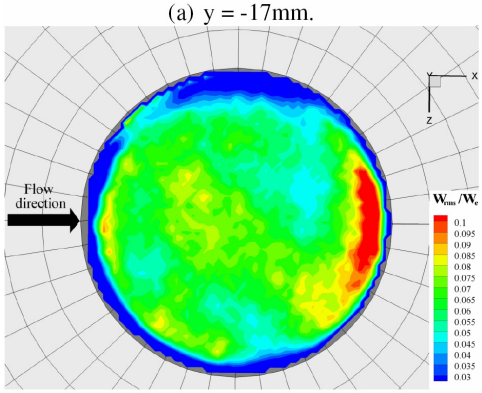

(b) y = -10mm.

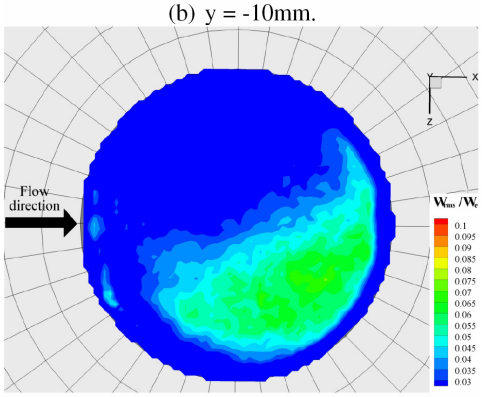

(c) y = -3mm.

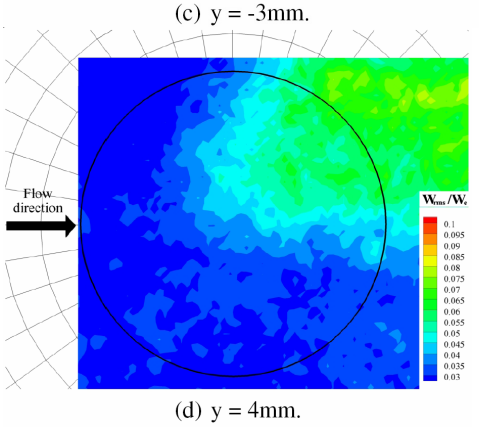

(d) y = 4mm.

Fig. 13. RMS values of W-velocity in different horizontal planes.

5 Tomographic PIV results

Fig. 14 shows slices at y = -3mm through two instantaneous velocity fields obtained from the tomographic PIV measurements. The large-scale flow pattern is similar to the mean flow pattern from the stereo PIV results, but it includes instantaneous turbulent motions. The out of plane component of the velocity, coded by the vector color, shows still the flow entering in the ”lower” downstream part of the cavity and exiting at the opposite side, indicating that the asymmetric flow has a rather steady character. The flow is populated by turbulent structures, better visible in Fig. 15, where the instantaneous vorticity iso-surface are shown for w = 1500 1/s.

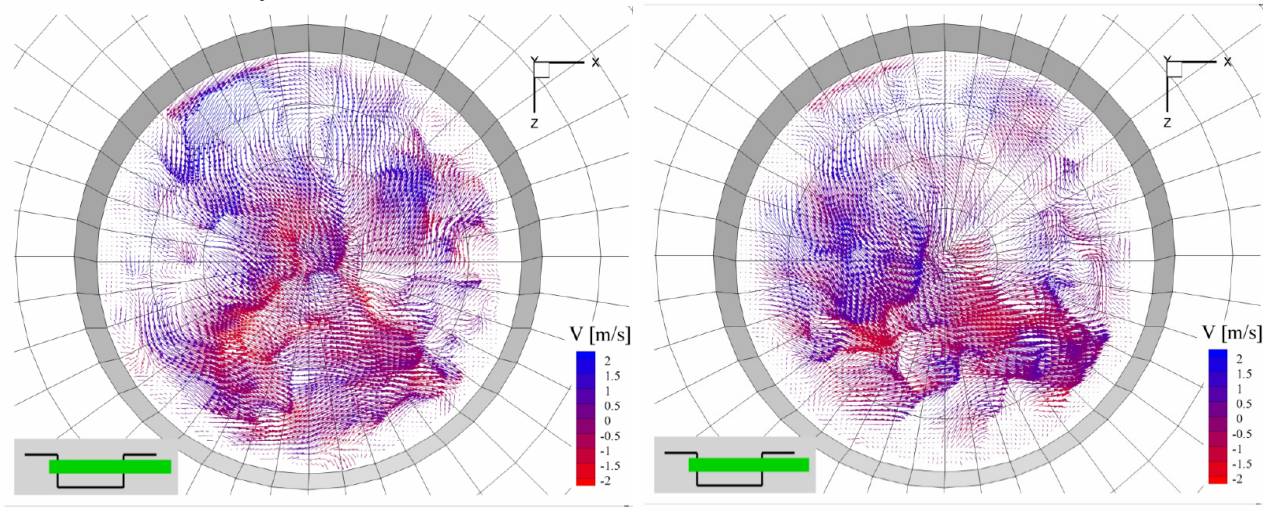

(a) Snapshot 1. (b) Snapshot 2.

Fig. 14 Slice through instantaneous velocity fields at y = -3mm.

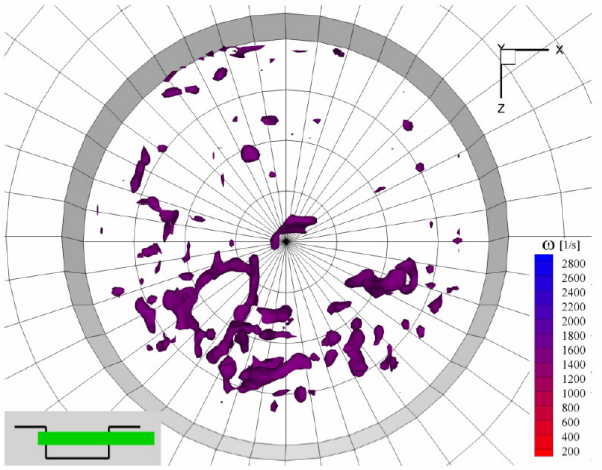

Fig. 15 Absolute vorticity ω.

One notices a higher density of vorticity in the ”lower” part in the images, where the flow enters. These are either vortices shed from the cavities leading edge, or structures coming from the turbulent boundary layer, which are convected inside the cavity's shear layer, but presumably it is a mixture of both effects. Instead, in the ”upper” part of the cavity, where slow fluid exits the cavity, weaker vertical structures are found. Further, a irregular distribution of vertical structures can be seen, which was also observed from the measurements in the vertical plane as described above. This indicates a more random instability mechanism in the cavity's shear layer, which is probably influenced by the turbulence properties of the thick incoming boundary layer.

6 Conclusion

The flow inside a circular cavity with and aspect ratio D/H=2 and a fully turbulent incoming boundary layer was studied using stereo and tomographic PIV. The instantaneous velocity fields from the stereo PIV results in the vertical plane show an irregular vortex shedding from the cavity's leading edge indicated by the irregular spacing of the identified vortices. This was observed in all instantaneous vector fields. The out of plane component of the mean velocity field shows the asymmetrical character of the flow, where the pattern can be divided in two parts, the downstream part close to the bottom wall and the upstream part including a part of the shear layer. The mean velocity fields at different locations parallel to the wall reveal a steady recirculation present in the cavity. Close to the bottom wall the center of the recirculation is located in the upstream part where $z > 0$. Moving further away from the bottom wall the center is displaced in clock-wise direction until a position opposite to the one close to the bottom wall. The streamlines indicate the form of the recirculation and show that the recirculation core line is vertical to the bottom wall for positions close to it and is tilted more and more in stream wise direction when moving out of the cavity. For planes inside the cavity, high turbulent activity is seen where the outer flow is entrained into the cavity, whereas the flow exhibits relatively low fluctuations where it moves outwards the cavity. For planes outside the cavity, high turbulence activity is found where the flow exits the cavity and interacts with the incoming boundary layer. The instantaneous velocity fields obtained by tomographic PIV measurements show the 3-dimensional flow pattern for an area inside the cavity. Vorticity iso-surfaces indicate flow structures which are present in the region where the flow enters the cavity, possibly shed from the cavities leading edge or coming from the turbulent boundary layer. A higher density of vortical structures is found in the ”lower” part ($z > 0$), where the flow enters into the cavity, whereas less structures are found in the ”upper” part.

Acknowledgements

This research project has been supported by a Marie Curie Early Stage Research Training Fellowship of the European Community's Sixth Framework Programme under contract number MEST CT 2005 020301.

References

1. Hiwada, M., Kawamura, T., Mabuchi, I., Kumada,M., Some Characteristics of the Flow Pattern and Heat Transfer past a Circular Cylindrical Cavity. *Bulletin of the JSME*, Vol. 26, No. 220, pp. 1744- 1752, 1983.
2. Dybenko, J., Hering, T., Savory, E., Turbulent Boundary Layer Flow over Circular cavities. *ICAS Hamburg,* n. 395, 2006.
3. Rossiter, J. E., Wind-Tunnel Experiment on the Flow over Rectangular Cavities at Subsonic and Transonic Speeds. *British ARC R&M,* No. 3428, 1964.
4. Sen, S.N., Acoustics - Waves and Oscillations. *Wiley Eastern Ltd.*, 1990.
5. Rona A., The acoustic resonance of rectangular and cylindrical cavities, *13th AIAA/CEAS Aeroacoustics Conference (28th AIAA Aeroacoustics Conference)*, 2007.
6. Elsinga GE, Van Oudheusden BW, Scarano F, Experimental assessment of tomographic-PIV accuracy. *13th international symposium on applications of laser techniques to fluid mechanics*, Lisbon, Portugal, paper 20.5, 2006.
7. G. E. Elsinga, F. Scarano, B. Wieneke, B. W. van Oudheusden, Tomographic particle image velocimetry, *Exp Fluids,* Vol. 41, p. 933947, 2006.
8. Wieneke B., Stereo-PIV using self-calibration on particle images, *Exp Fluids,* Vol. 39, p. 267-280, 2005.
9. Zou J., Adrian R. J., Balachandar S., Kendall T. M., Mechanisms of generating coherent packets of hairpin vortices in channel flow, *J. Fluid Mech.* 387, pp. 353-396, 1999.